Ultrasound in Med. & Biol., Vol. 45, No. 2, pp. 440−451, 2019

0301-5629/$ - see front matter

https://doi.org/10.1016/j.ultrasmedbio.2018.07.009

● *Original Contribution*

NON-INVASIVE QUANTITATIVE ASSESSMENT OF MUSCLE FORCE BASED ON ULTRASONIC SHEAR WAVE ELASTOGRAPHY

JING LIU,* ZHIHUI QIAN,* KUNYANG WANG,† JIANAN WU,* ALI JABRAN,† LUQUAN REN,* and LEI REN*,†
* Key Laboratory of Bionic Engineering, Ministry of Education, Jilin University, Changchun, China; and † School of Mechanical, Aerospace and Civil Engineering, University of Manchester, Manchester, United Kingdom

(*Received* 15 *May* 2018; *revised* 3 *July* 2018; *in final from* 13 *July* 2018)

Abstract—The objective of this study was to investigate the feasibility of using shear wave elastography (SWE) to indirectly measure passive muscle force and to examine the effects of muscle mass and scan angle. We measured the Young's moduli of 24 specimens from six muscles of four swine at different passive muscle loads under different scan angles (0°, 30°, 60° and 90°) using SWE. Highly linear relationships between Young's modulus *E* and passive muscle force *F* were found for all 24 muscle specimens at 0° scan angle with coefficients of determination R^2 ranging from 0.984 to 0.999. The results indicate that the muscle mass has no significant effect on the muscle *E*−*F* relationship, whereas *E*−*F* linearity decreases disproportionately with increased scan angle. These findings suggest that SWE, when carefully applied, can provide a highly reliable tool to measure muscle Young's modulus, and could be used to assess the muscle force quantitatively. (E-mail: lei.ren@manchester.ac.uk) © 2018 The Author(s). Published by Elsevier Inc. on behalf of World Federation for Ultrasound in Medicine & Biology. This is an open access article under the CC BY-NC-ND license. (http://creativecommons.org/licenses/by-nc-nd/4.0/).

Key Words: **Shear wave elastography, Muscle Young's modulus, Muscle passive force, Muscle mass, Probe scan angle.**

INTRODUCTION

Muscles play the role of an actuator in the human musculoskeletal system, allowing the performance of a range of complex movements. Determining individual muscle force is fundamentally important for many fields, such as biomechanics, orthopedics, robotics and rehabilitation engineering (Huijing 1999; Hug et al. 2015). Muscle force of a single muscle is traditionally determined either by direct measurements or by indirect calculations. Direct measurements have mostly been performed on cadavers and animals, but rarely *in vivo* because of the ethical concerns, as they require invasive tests to be conducted on a large subject population. As for the indirect calculations, electromyography (EMG) (Hylander et al. 2000; Lloyd and Besier 2003; Ziai and Menon 2011) and musculoskeletal models (Ackland et al. 2012; Erdemir et al. 2007; Modenese and Phillips 2012) have been used extensively. EMG measures the electrophysiologic activity of muscles, and this activity is used as a metric for quantifying the force exerted by the muscles. An EMG signal is a superposition of the action potentials of multiple muscles during contraction. This makes it difficult to obtain an EMG signal that corresponds exclusively to a single muscle (Buchanan et al. 2004). Furthermore, the failure of EMG to measure muscle passive force and the fact that the relationship between surface EMG signal and muscle force is sensitive to neuromuscular fatigue limit its use for measuring muscle force (Edwards and Lippold 1956). On the other hand, various musculoskeletal models based on mathematical descriptions of muscle contraction dynamics (Hill 1938; Huxley and Niedergerke 1954) have been developed to estimate individual muscle forces. However, because of the large assumptions introduced in these models, their validity remains uncertain. Thus far, non-invasive assessment of muscle force remains one of the grand challenges in biomechanics (Hug et al. 2015).

Elastography is a family of non-invasive techniques for real-time measurement of tissue elasticity (Nightingale et al. 2003; Turgay et al. 2006; Urban et al. 2013). Some of these techniques, such as vibration elastography imaging and magnetic resonance elastography (MRE), have been used to quantify muscle force. Levinson et al. (1995) measured muscle elasticity

Address correspondence to: Lei Ren, School of Mechanical, Aerospace and Civil Engineering University of Manchester, Manchester, UK M13 9PL. E-mail: lei.ren@manchester.ac.uk

using vibration elastography and found a linear correlation between Young's modulus of the quadriceps femoris muscle and the applied load. Dresner et al. (2001) used MRE to determine the quantitative relationship between the shear elastic modulus and passive force in bovine muscles. Although MRE yielded superior elasticity data for a single muscle or muscle group (Debernard et al. 2011a, 2011b), its use is limited by its high cost and poor real-time application (Anderson et al. 2016; Weickenmeier et al. 2018).

Ultrasound-based elastography techniques, in general, have been compared with MRE and have exhibited good agreement for a wide range of tissues and phantoms (Bensamoun et al. 2008; Dutt et al. 2000; Oudry et al. 2009). One such technique is shear wave elastography (SWE), which has been used to quantitatively characterise the mechanical parameters of tissues (Bercoff et al. 2004; Haen et al. 2017; Liu et al. 2017; Palmeri et al. 2008; Sarvazyan et al. 1998). SWE operates by subjecting the tissue to mechanical perturbations by using the acoustic radiation force generated by the ultrasonic beams. This induces shear waves that propagate within the tissue. As the shear waves propagate, they are captured by the ultrasound transducer at an ultrafast frame rate. Algorithms such as the cross-correlation algorithm are then used to estimate the propagation speed of these shear waves at each pixel. This shear wave speed (V_s) is related to the shear elastic modulus (μ) *via* a square relationship defined by muscle mass density (ρ), which is often assumed to be 1000 kg/m^3:

$$\mu = \rho V_s^2 \tag{1}$$

For biological tissues, Young's modulus is approximately triple its shear modulus, under the assumption that the tissue is isotropic, homogeneous and quasi-incompressible. These assumptions have been reported to hold true for hepatic tissues, leading to the relatively high use of SWE in screening for such conditions as liver fibrosis, as well as for differentiating cirrhotic from healthy liver tissue (Anyona Sande et al. 2017; Kim et al. 2018; Mulabecirovic et al. 2018). Theoretically, these assumptions would rule out the use of SWE on skeletal muscles because of their tissue anisotropy. However, Eby et al. (2013) reported a strong linear relationship between muscle shear modulus and muscle Young's modulus. In several studies, SWE has been successfully used to quantify muscle Young's modulus (Bouillard et al. 2011; Koo et al. 2014; Maïsetti et al. 2012; Nordez and Hug 2010; Nordez et al. 2008; Tran et al. 2016). Some attempts have also been made to indirectly evaluate muscle forces based on muscle elasticity using SWE (Bouillard et al. 2011; Kim et al. 2018; Koo et al. 2013). Koo et al. (2013) measured the shear modulus of two chicken leg muscles of similar mass using SWE under *in vitro* loading condition and reported a strong linear relationship between muscle elasticity and muscle force. This suggests that SWE may be a promising method for evaluation of muscle force indirectly.

Little, however, is known about whether this strong linear relationship holds for muscles of different masses and how muscle mass and ultrasound wave orientation affect this linearity. A systematic study is yet to be found in the literature that investigated the effects of muscle mass and ultrasound wave orientation on the relationship between muscle elasticity and muscle force. This is crucial not only to the design of future measurements that determine the elasticity and force of anisotropic and inhomogeneous muscle tissues (Gennisson et al. 2003), but also to the clinical use of SWE.

The objective of this study was to examine the relationship between SWE-measured Young's modulus (E) and the passive muscle force (F) of different porcine muscles across a large mass range during *in vitro* loading measurements. We systematically determined the repeatability of the measured Young's modulus and the effect of muscle mass and probe scan angle, that is, the angle between the ultrasonic beam and muscle fibre, on the $E-F$ relationship. This knowledge will allow us to better understand the key contributing factors when using SWE to quantify passive muscle load.

METHODS

Muscle specimen preparation

Twenty-four muscle specimens were dissected from four fresh and healthy swine, obtained immediately post mortem, with a mean mass ± SD of 139 ± 5 kg and mean age of 1.5 ± 0.2 y. To avoid the cluster effect of the muscle cross-sectional area resulting from the consistency in the muscle mass of samples, we dissected 24 muscle samples from six muscles with different masses, namely, brachialis, peroneus tertius, common digital extensor, tibialis anterior, extensor carpi radialis and gastrocnemius (see Table 1). This study was approved by the Institutional Review Board Committee of Jilin University, Changchun, China (No. 20170329). The samples were sprayed with cold physiologic saline solution throughout preparation and test procedures.

Test device

Before measurement, one end of the muscle (tendon) was clamped in the fixture while calibration weights were applied to the other end *via* a pulley−cable system (see Fig. 1). Before the tensile loading test, the ultrasound transducer was placed over one-half of the muscle specimens to prevent stress concentration arising

Table 1. Muscle mass of all the 24 specimens

Muscle	Swine A (g)	Swine B (g)	Swine C (g)	Swine D (g)
Brachialis	125.29	120.88	116.30	124.10
Peroneus tertius	52.46	39.53	35.94	45.60
Common digital extensor	26.00	18.25	21.63	23.22
Tibialis anterior	105.22	97.90	89.71	101.32
Extensor carpi radialis	152.00	142.85	134.64	148.64
Gastrocnemius	68.16	65.70	61.21	66.78

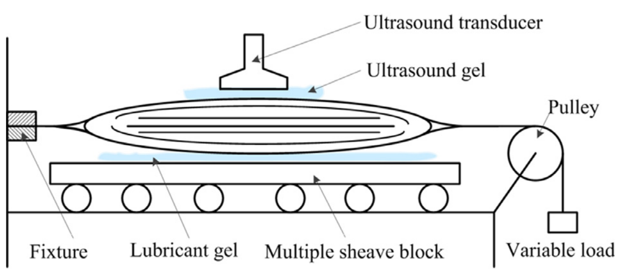

Fig. 1. Schematic of the experimental setup used to apply passive force (F) to the distal end of the muscle. A gel lubricant was applied on the table surface to reduce friction.

from the fixation of muscle specimens at both ends. The transducer was then held by an operator's hand. The pressure between the transducer and muscle specimens was kept minimal and constant by repositioning the transducer to avoid the artefact of an elastic image owing to the excessive probe pressure (see Fig. 1).

Elasticity measurements

Young's moduli of the swine specimens were measured with an Aixplorer ultrasound scanner (Aixplorer, SuperSonic Imaging, Aix-en-Provence, France) in the SWE mode using the musculoskeletal pre-set to allow large shear modulus values to be measured. A linear transducer of 15−4 MHz was used in this study. First, a brief B-mode ultrasound examination was done to confirm the muscle fibre orientation of the muscle specimen. Instinctively, alignment of the transducer with respect to the long axis of the muscle fibre was manipulated, and the location of the probe was defined as the initial position of scan angle 0°. The probe rotated 30°, 60° and 90° in turn, and these positions were defined as the measuring positions of 30°, 60° and 90°, respectively. Subsequently, shear wave elastography generated colour-coded images where *blue, green, orange* and *red* represented Young's modulus values from low to high (see Fig. 2).

For each tested muscle, SWE was performed and the square-shaped elastography window (region of interest) position was fixed, except at the upper and lower borders (risk of boundary effect) (Brandenburg et al. 2014). The size of the elastography window was set as 10×10 mm^2 (Kelly et al. 2017; Le et al. 2017; Umegaki et al. 2015), as illustrated in Figure 2. Using Q-BOX (a circle with a diameter of 6 mm) (Kot et al. 2012), a built-in quantitative measuring tool, the maximum, minimum and mean Young's moduli were measured. The mean Young's modulus was used for the data analysis in this study. SWE measurements were conducted at 20 different applied loads from 0 to 18.0 times the muscle weight (BW). At each load, the Young's modulus test was performed at four different scan angles: 0°, 30°, 60° and 90°. The elastography window was first allowed to stabilize for 5 s, and then the elastography image was acquired. The Young's modulus measurement was repeated three times at each scan angle. Because the elastography window was located at the same position throughout the measurement, the measured data obtained in the tests for different loads and scan angles can be compared directly.

Data analysis

All data analyses were performed using the IBM Statistical Package for the Social Sciences (SPSS) Statistics software, Version 13.0 (IBM, Armonk, NY, USA). Continuous variables were expressed as means ± SD. The 95% confidence interval (95% CI) and intra-class correlation coefficient (1, 1) ($ICC_{1,1}$) were used to measure and assess the reliability of the Young's modulus test results. Generally, $ICC_{1,1}$ values within the ranges 0−0.40, 0.41−0.6, 0.61−0.79 and 0.8−1.0 indicate poor, moderate, good and excellent reliability, respectively (Cohen 1968).

The $E-F$ relationship between the Young's modulus and the passive muscle force of each tested muscle at each loading cycle was analysed by least-squares linear fitting using the equation

$$E = E_0 + kF \quad (2)$$

where E is the Young's modulus of the muscle under a passive force F. E_0 represents the Young's modulus of the slack muscle, and k is the change rate of the Young's modulus with respect to the normalised muscle force (passive muscle force divided by muscle weight). Based on measured Young's modulus and muscle force data, E_0, k and the coefficient of determination (R^2) of each regression line were calculated.

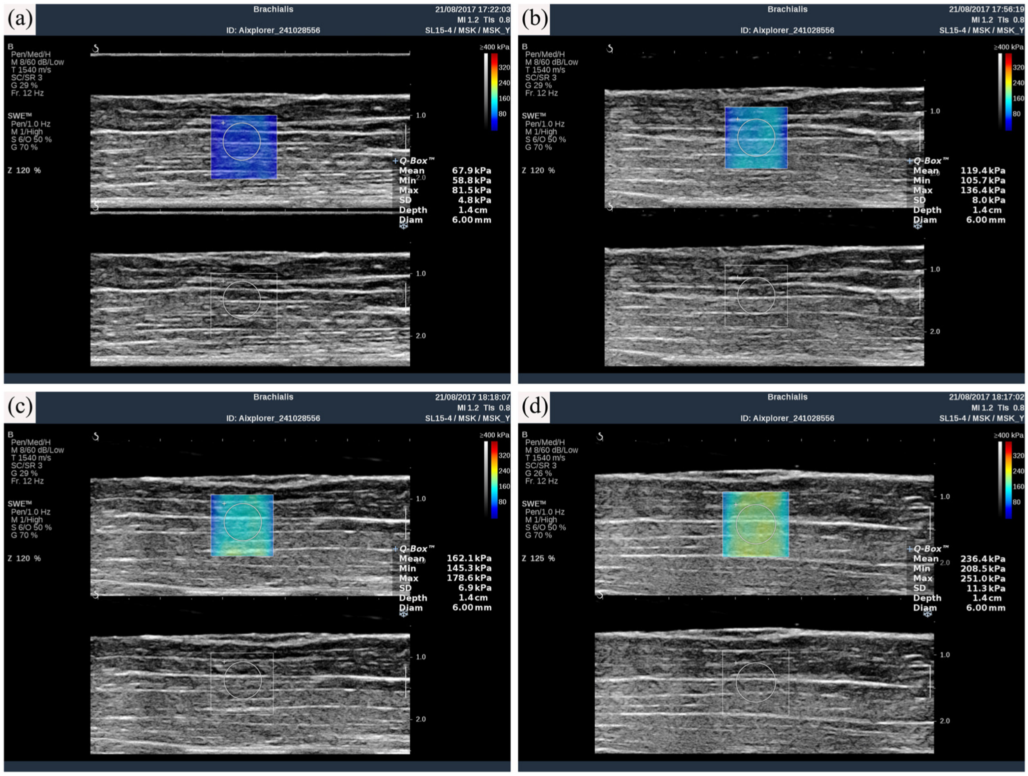

Fig. 2. Examples of elastography images of the brachialis muscle at scan angle 0˚ subjected to a passive tensile force of 0 BW (a), 6 BW (b), 12 BW (c) and 18 BW (d). BW = weight of the muscle.

RESULTS

Repeatability analysis of Young's modulus measurement

The test−retest reliability results of the SWE measurement of the 24 muscle specimens from four swine at scan angle $\alpha = 0^\circ$ are outlined in Table 2. It can be seen that the $ICC_{1,1}$ ranges from 0.985 to 0.999 and the 95% CI is between 0.969 and 0.999 for all muscle specimens tested. This indicates that the SWE-measured muscle Young's modulus exhibited very high reliability.

Relationship between Young's modulus and muscle force

Figure 3 illustrates the fitting curve of the Young's modulus of the brachialis of swine A versus passive loading force data at scan angle $\alpha = 0^\circ$ and reveals a strong linear relationship between them. The coefficient of determination (R^2) is 0.998. Figure 4 illustrates the linear regression fitting results of the $E-F$ relationship for all six muscles and all four swine. The coefficients of determination (R^2) obtained are listed in Table 2. It can be seen that very strong linear $E-F$ relationships were found in all 24 muscle specimens tested with coefficients of determination (R^2) ranging from 0.984 to 0.999 (see Fig. 4).

Effect of muscle mass on E−F relationship

Figure 4 also reveals that for the same type of muscle, the linear relationship between the Young's modulus and passive loading force is similar for the different swine. The calculated intercept E_0 and slope k of the regression lines for all 24 muscle specimens are listed in Table 3. Figure 5 illustrates the change in intercept E_0 and slope k with respect to muscle mass for all specimens. It can be found that for the same muscle, the E_0 or k values of the four swine are very similar. There is no significant difference between E_0 or k and the mass of muscle itself. For all six muscles tested, E_0 is in the range 46.200−73.396 kPa, and k is within the range 8.444−9.835 kPa, with only one exception, the peroneus tertius, for which the k value (5.874−6.057 kPa) is lower than those of other muscles.

Effect of scan angle on E−F relationship

In Figure 6 are the elastography images of the brachialis muscle of swine A at scan angles 0˚, 30˚, 60˚ and 90˚. It can be seen that the measured minimum, maximum and mean Young's moduli all decrease drastically with increasing scan angle. The change in the mean Young's modulus with respect to scan angle is illustrated in Figure 7a. It can be seen that the Young's modulus peaks when the ultrasonic beam is parallel to the muscle

Table 2. Reliability of Young's modulus ($ICC_{1,1}$) and coefficients of determination (R^2) of linear regression fit of Young's modulus versus passive muscle force data of all 24 muscle specimens at 0° scan angle

Muscle	Swine A			Swine B			Swine C			Swine D		
	$ICC_{1,1}$	95% CI	R^2	$ICC_{1,1}$	95% CI	R^2	$ICC_{1,1}$	95% CI	R^2	$ICC_{1,1}$	95% CI	R^2
Brachialis	0.995	(0.990−0.998)	0.99788	0.995	(0.991−0.998)	0.99498	0.997	(0.994−0.999)	0.99581	0.999	(0.997−0.999)	0.99872
Peroneus tertius	0.987	(0.973−0.994)	0.98373	0.992	(0.984−0.997)	0.99204	0.985	(0.969−0.994)	0.98519	0.997	(0.994−0.999)	0.99589
Common digital extensor	0.994	(0.988−0.998)	0.99620	0.991	(0.981−0.996)	0.99525	0.995	(0.990−0.998)	0.99536	0.998	(0.996−0.999)	0.99844
Tibialis anterior	0.995	(0.989−0.998)	0.99539	0.996	(0.992−0.998)	0.99245	0.995	(0.989−0.998)	0.99076	0.998	(0.995−0.999)	0.99713
Extensor carpi radialis	0.996	(0.991−0.998)	0.99261	0.995	(0.989−0.998)	0.99533	0.995	(0.989−0.998)	0.99538	0.998	(0.995−0.999)	0.99780
Gastrocnemius	0.995	(0.990−0.998)	0.99532	0.995	(0.989−0.998)	0.99640	0.995	(0.989−0.998)	0.99482	0.999	(0.997−0.999)	0.99866

CI = confidence interval; $ICC_{1,1}$ = intra-class correlation coefficient.

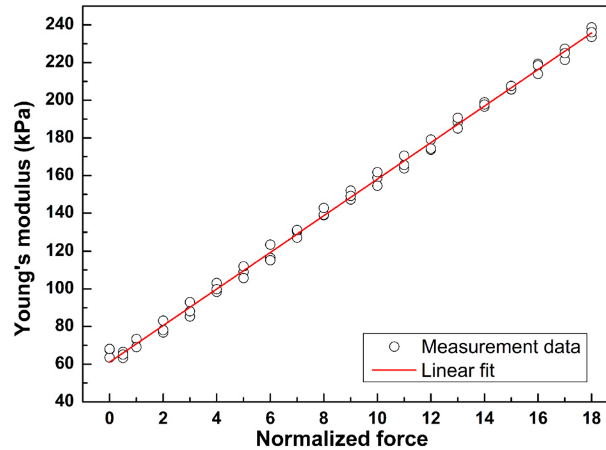

Fig. 3. Linear curve fitting for Young's modulus of the brachialis of swine A versus muscle force.

fibre ($\alpha = 0°$) and rapidly decreases when the probe diverges away from the orientation of the muscle fibre. Figure 8 illustrates the linear fitting results of the $E-F$ relationship of the brachialis muscle of swine A at scan angles 0°, 30°, 60° and 90°. It can be seen that the measurement data are more scattered away from the line with increased scan angle. The calculated coefficient of determination (R^2) in Figure 7b decreases drastically when scan angle increases. The calculated coefficients of determination (R^2) of all 24 muscle specimens at scan angles 30 °, 60° and 90° are listed in Table 4. The same trends are observed for all muscles tested, suggesting that increasing the probe scan angle significantly deteriorates the linearity of the muscle $E-F$ relationship.

DISCUSSION

In this study, excellent repeatability was observed when measuring the muscle Young's modulus using ultrasound SWE. The experimental setup used here achieved high reproducibility, probably because we carefully followed the manufacturer's guidelines (SuperSonic Imagine 2016), which emphasise the importance of stabilising the transducer and minimising stress artefacts for accurate data acquisition. To achieve the former, the probe's position was carefully maintained by the operator, and a gel lubricant was used between the probe and the muscle. For the latter, the pressure between the probe and the muscle was kept constant and minimal by adjusting the probe up and down. It should be noted that this experience contrasts with the findings of Alfuraih et al. (2018), who recommended placing the probe in direct contact with the skin for more reliable results rather than using a gel lubricant.

Previous studies attempted to use ultrasound elastography to quantify biomechanical characteristics of skeletal muscles. For example, Maïsetti et al. (2012)

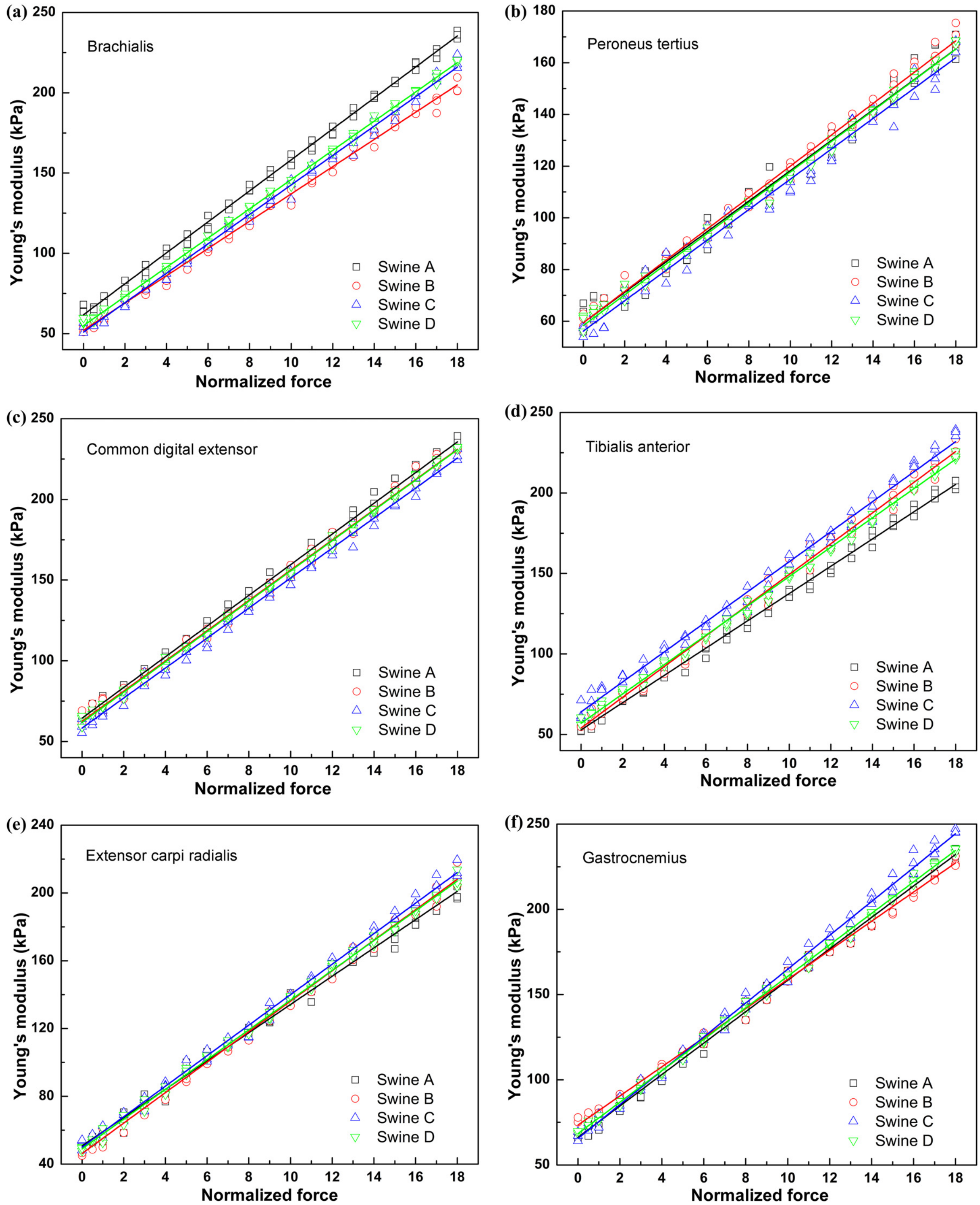

Fig. 4. Linear fitting results of the $E-F$ relationship for all six muscles and all four swine: brachialis (a), peroneus tertius (b), common digital extensor (c), tibialis anterior (d), extensor carpi radialis (e), gastrocnemius (f).

reported a non-linear relationship between the shear modulus and the tendon length of some human leg muscles during passive ankle dorsiflexion and plantar flexion. They suggested that muscle shear modulus could be used to indirectly assess passive muscle force. Similarly, Bouillard et al. (2011) reported a strong relationship ($R^2 = 0.951-0.997$) between the muscle shear modulus and muscle contraction torque of two finger muscles during isometric abduction by neglecting the contributions of the other muscles. Recently,

Table 3. Calculated linear regression parameters: Intercept E_0 and slope k for all 24 specimens

Muscle	Swine A		Swine B		Swine C		Swine D	
	E_0 (kPa)	k (kPa/BW)	E_0 (kPa)	k (kPa/BW)	E_0 (kPa)	k (kPa/BW)	E_0 (kPa)	k (kPa/BW)
Brachialis	61.1100	9.6000	52.0682	8.4900	50.9153	9.1700	54.8990	9.1040
Peroneus tertius	59.4613	5.8793	59.4215	6.0570	56.2057	5.8744	58.3629	5.9370
Common digital extensor	64.4189	9.5154	58.2913	9.2990	62.4598	9.3687	61.7234	9.3944
Tibialis anterior	52.7903	9.3290	62.9610	8.5700	53.9970	9.5417	56.9164	9.1148
Extensor carpi radialis	50.7604	8.4440	49.9485	9.0000	46.1999	8.9950	48.9696	8.7810
Gastrocnemius	66.1400	9.2230	73.3962	8.6460	65.5196	9.8350	68.3531	9.2347

BW = muscle weight.

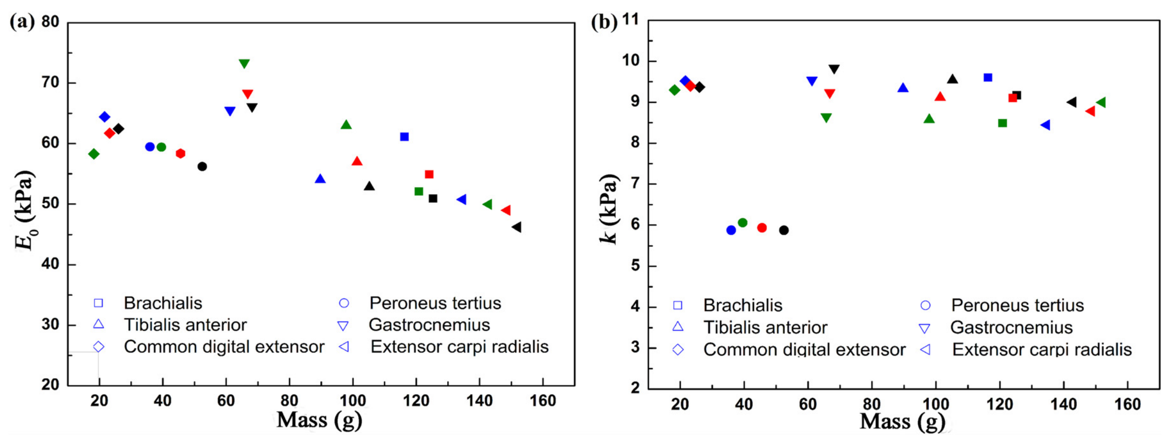

Fig. 5. Linear regression parameters of the $E-F$ relationship versus muscle mass Young's modulus of slack muscle E_0 (a), and the change rate k of Young's modulus with respect to normalised muscle force (b). Symbols for swine A are *blue*, for swine B *green*, for swine C *black* and for swine D *red*.

Koo et al. (2013) reported a linear $E-F$ relationship ($R^2 = 0.971-0.999$) between muscle shear modulus and passive force on two chicken leg muscles of similar mass in a cadaveric study using SWE. However, the consistency in the muscle mass may have led to cluster effects in the cross-sectional area of the muscle, which is detrimental to analysis of the relationships between muscle pennation angle, cross-sectional area and shear modulus. Therefore, investigations into the effect of muscle mass are useful in examining the feasibility of the indirect muscle force evaluation method using SWE across a wider range of muscle mass and size.

In this study, we examined the $E-F$ relationship of six swine muscles with muscle mass ranging from 18.25 to 152 g using ultrasound SWE. We found that there exists a very strong linear relationship ($R^2 = 0.984$ 0.999) between the Young's modulus and the muscle force for all 24 specimens tested, with muscle mass across almost one order of magnitude, strongly suggesting that ultrasound SWE could be used to quantify passive muscle force of different masses and sizes. Interestingly, we also found that the two linear regression parameters of the $E-F$ relationship, that is, the intercept E_0 (or slack muscle Young's modules) and the slope k (or change rate of Young's modulus with respect to normalised muscle force), do not change significantly with muscle mass. For all specimens tested in this study, E_0 ranged from 45 to 75 kPa, and k was in the range 8−10 kPa, the only exception being the k value of the peroneus tertius muscle, possibly because of the difference in muscle morphology and material properties. Nevertheless, the general linear $E-F$ relationship revealed in this study could provide a predictive model to indirectly estimate muscle force based on ultrasound SWE data. Although the normalised muscle force, rather than the absolute muscle force, is involved in the linear relationship, with the emerging ultrasound techniques capable of measuring individual muscle volume (Barber et al. 2009; Schless et al. 2018), we could readily obtain the weight of individual muscles based on muscle density (Snyder et al. 1975) in the near future and, thereby, the absolute muscle force. In this scenario, the general linear relationship between the muscle elasticity and the normalised muscle force found in this study will provide a very useful clinical tool to evaluate the individual muscle force using ultrasound SWE. This work is novel and clinically important as most previous studies focused on the absolute muscle force and found that it presents quite

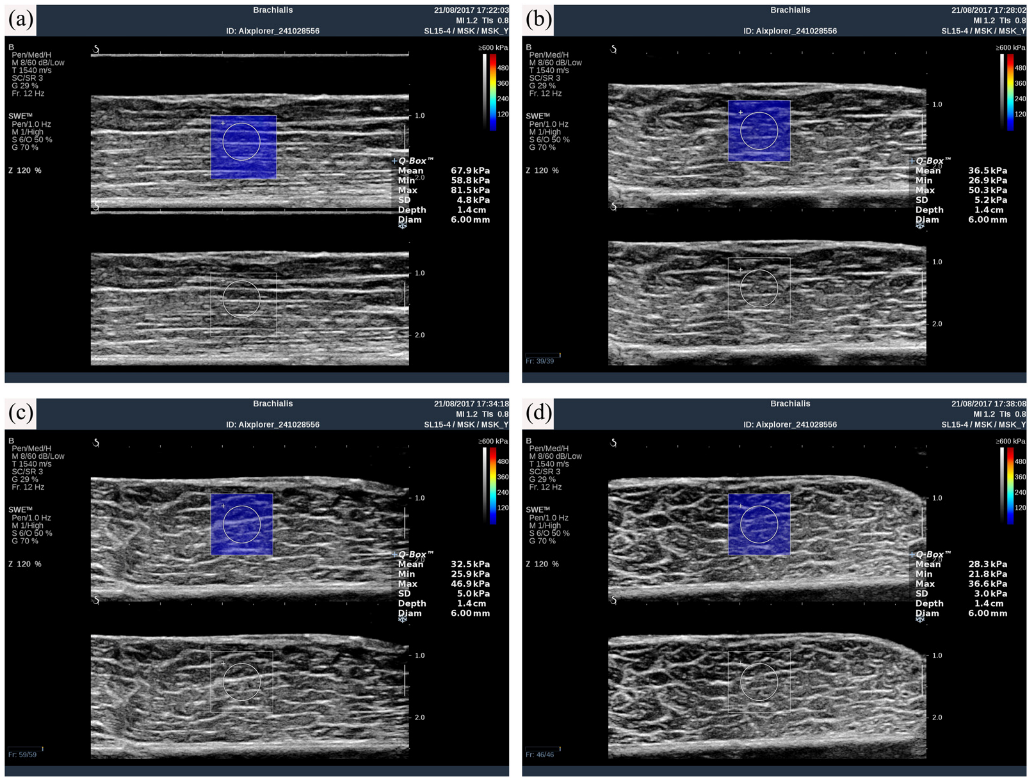

Fig. 6. Example elastography images of the brachialis muscle of swine A at different scan angles: 0˚ (a), 30˚ (b), 60˚ (c), 90˚ (d).

different linear relationships with muscle elasticity for different muscles, which makes clinical application quite challenging.

Our results indicated that the probe scan angle (the angle between the ultrasound probe and the muscle fibre) has a significant effect on the muscle $E-F$ relationship. Increasing the scan angle significantly decreases the linearity of the $E-F$ relationship. The linear coefficient of determination (R^2) decreases disproportionally with increased scan angle. To the best of our knowledge, this has not been reported before. Considering the complex morphology and architecture of skeletal muscles, caution must be used in future muscle SWE measurements. The ultrasonic probe should be placed parallel to the muscle fibre to produce high-quality data. This is supported by observations in previous studies. For example,

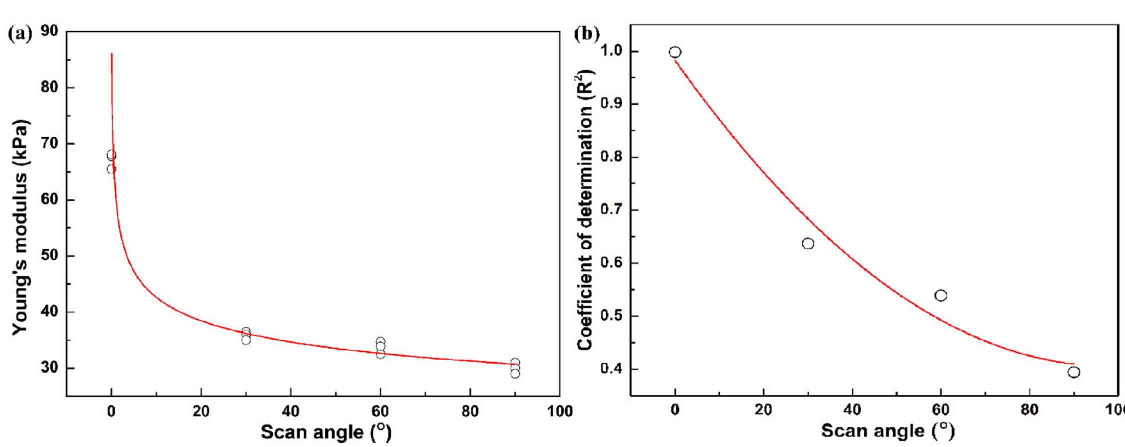

Fig. 7. Measured Young's modulus (a) and calculated coefficient of determination (R^2) of linear fit of $E-F$ relationship (b) for the brachialis muscle of swine A at different scan angles: 0˚, 30˚, 60˚ and 90˚.

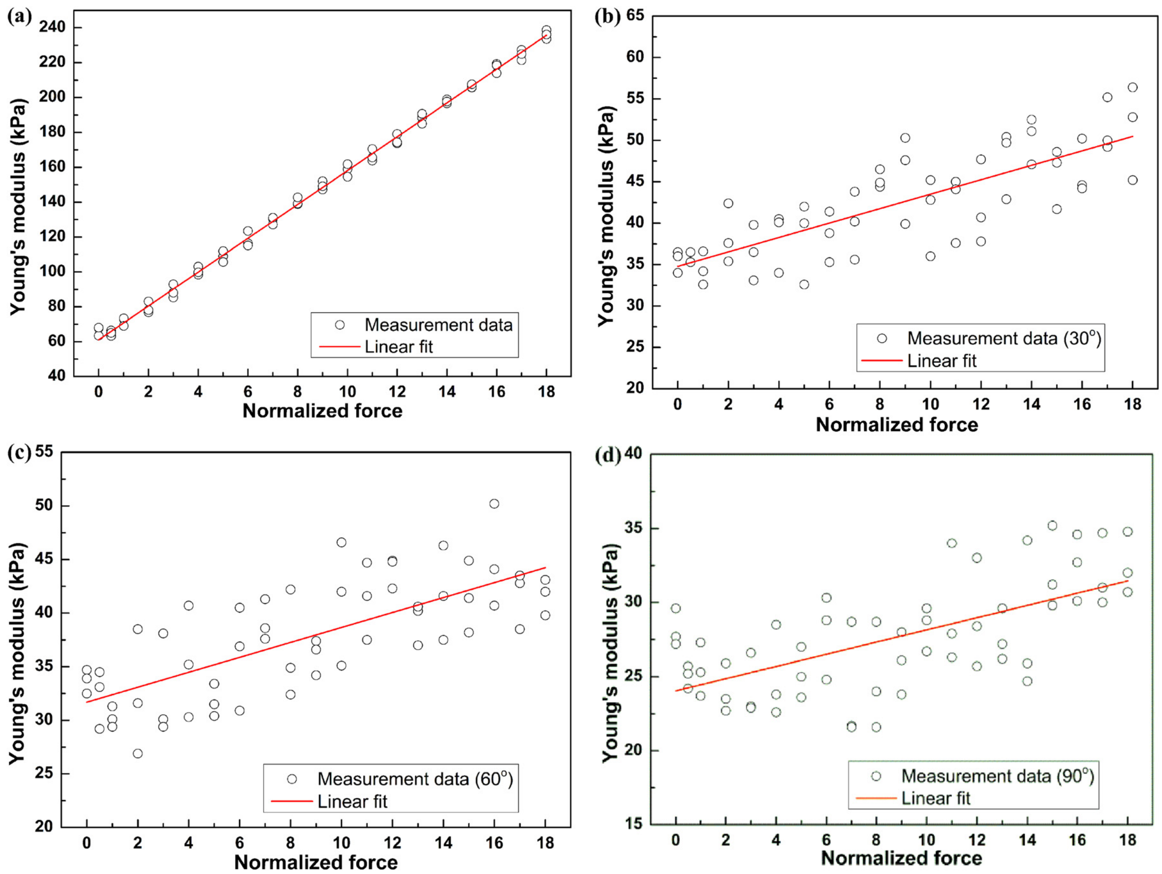

Fig. 8. Linear curve fitting results of the $E-F$ relationships of the brachialis muscle of swine A at different scan angles: 0° (a), 30° (b), 60° (c) and 90°(d).

Gennisson et al. (2003) found that shear waves propagate much more readily along beef muscle fibres longitudinally than propagating perpendicularly or in other orientations. Eby et al. (2013) reported a strong linear relationship between muscle shear modulus and Young's modulus when the ultrasound probe was parallel to the

Table 4. Coefficients of determination (R^2) of the linear regression fit for Young's modulus versus passive muscle force data obtained for all 24 muscle specimens at different scan angles

Muscle	Scan angle, α	Swine A	Swine B	Swine C	Swine D
Brachialis	30°	0.63686	0.62356	0.61534	0.65432
	60°	0.53888	0.52369	0.52690	0.51236
	90°	0.39424	0.38460	0.40123	0.38956
Peroneus tertius	30°	0.64895	0.65230	0.65489	0.64210
	60°	0.56231	0.56423	0.55410	0.54159
	90°	0.37569	0.36952	0.39465	0.39621
Common digital extensor	30°	0.69852	0.68421	0.68745	0.68921
	60°	0.56320	0.55302	0.63590	0.63762
	90°	0.35698	0.34895	0.35621	0.36823
Tibialis anterior	30°	0.68520	0.67531	0.68360	0.65301
	60°	0.52130	0.54036	0.54219	0.52930
	90°	0.38265	0.36258	0.34269	0.33448
Extensor carpi radialis	30°	0.63589	0.65420	0.68231	0.67530
	60°	0.54123	0.53962	0.55662	0.54660
	90°	0.35520	0.36621	0.38410	0.36423
Gastrocnemius	30°	0.65209	0.64780	0.63452	0.68421
	60°	0.52369	0.52486	0.53621	0.53320
	90°	0.34699	0.39951	0.36552	0.35110

muscle fibres, but the shear waves did not propagate well at 45° and in the perpendicular orientation. This may be due to muscle anisotropy where Young's modulus varies along different directions. Moreover, the viscoelasticity of muscle tissue may contribute as well because most ultrasound transducers do not account for tissue viscoelasticity when calculating Young's modulus using SWE.

There are some limitations to this study. First, the accuracy of using ultrasound SWE to measure muscle Young's modulus is yet to be fully validated. Koo et al. (2013) compared SWE-measured shear modulus with reference values using an elasticity QA phantom for chicken muscles. However, the shear modulus was in a very small range (2.7−26.7 kPa), and a more comprehensive validation for larger shear modulus is required. In addition, we assumed a linear relationship between muscle shear modulus and Young's modulus based on the previous study by Eby et al. (2013) on swine muscles. A more thorough investigation is required to examine how muscle anisotropy, viscoelasticity and morphology affect the relationships found in this study. Furthermore, only the passive muscle forces on cadaveric specimens were investigated here. Studies are needed to examine the *in vivo* muscle $E-F$ relationship during different motor activities. Additionally, the elastic modulus obtained using the ultrasound probe is the property of a small local area within the muscle. The shear wave speed may be dependent on the local compositional, structural and mechanical properties of the tissue. Therefore, we selected the central part of the muscle belly as in previous studies (Eby et al. 2015; Hirata et al. 2016; Kentaro et al. 2012; Leonardis et al. 2017; Miyamoto et al. 2015; Umegaki et al. 2015) to report the muscle data. Finally, to be clinically useful, the SWE-based method needs to be examined in human specimens and patients. It was found that some swine organs and tissues are very similar to human organs and tissues in terms of biomechanical characteristics and material properties (Bhatia et al. 2012; Choi et al. 2014; Itoh et al. 2006; Kwak et al. 2011; Park et al. 2009; Zhi et al. 2008). It would be interesting to examine in future studies the linearity of the $E-F$ relationship of human muscles and to determine if the E_0 and k values of human muscles are in ranges to those of swine muscles.

CONCLUSIONS

In this study, we measured the Young's moduli of 24 specimens from six muscles of four swine at different passive muscle loads using ultrasound SWE and rigorously examined the repeatability of the measured Young's modulus, the $E-F$ relationship and the effects of muscle mass and probe scan angle on the $E-F$ relationship. It was found that ultrasound SWE provides a highly reliable and reproducible technique to measure muscle Young's modulus. There exists a very strong linear relationship between muscle Young's modulus and passive muscle force for all specimens tested across a large of range of muscle mass. It was found that the E_0 and k values of almost all muscles are in a very similar range, suggesting that the linear relationship revealed in this study could provide a predictive model to quantify passive muscle force for muscles of different masses and sizes. Moreover, it was found that the probe scan angle has a significant effect on the linearity of the $E-F$ relationship. Caution should be used in future muscle measurements using ultrasound SWE.

Acknowledgments—This research was supported by the National Natural Science Foundation of China (Project Nos. 51475202 and 51675222), the Postdoctoral Science Foundation of China (Project No. 2016 M601381), the National Key Research and Development Program of China (Project No. 2016 YFE0103700) and the Science and Technology Development Planning Project of Jilin Province (No. 20180101068 JC).

REFERENCES

Ackland DC, Lin YC, Pandy MG. Sensitivity of model predictions of muscle function to changes in moment arms and muscle−tendon properties: A Monte-Carlo analysis. J Biomech 2012;45:1463–1471.

Alfuraih AM, O'Connor P, Hensor E, Tan AL, Emery P, Wakefield RJ. The effect of unit, depth, and probe load on the reliability of muscle shear wave elastography: Variables affecting reliability of SWE. J Clin Ultrasound 2018;46:108–115.

Anderson AT, Van Houten EEW, McGarry MDJ, Paulsen KD, Holtrop JL, Sutton BP, Georgiadis JG, Johnson CL. Observation of direction-dependent mechanical properties in the human brain with multi-excitation MR elastography. J Mech Behav Biomed Mater 2016;59:538–546.

Anyona Sande J, Verjee S, Vinayak S, Amersi F, Ghesani M. Ultrasound shear wave elastography and liver fibrosis: A Prospective Multicenter Study Basic Study. World J Hepatol 2017;8:38–47.

Barber L, Barrett R, Lichtwark G. Validation of a freehand 3-D ultrasound system for morphological measures of the medial gastrocnemius muscle. J Biomech 2009;42:1313–1319.

Bensamoun SF, Wang L, Robert L, Charleux F, Latrive JP, Ho Ba Tho MC. Measurement of liver stiffness with two imaging techniques: Magnetic resonance elastography and ultrasound elastometry. J Magn Reson Imaging 2008;28:1287–1292.

Bercoff J, Tanter M, Fink M. Supersonic shear imaging: A new technique for soft tissue elasticity mapping. IEEE Trans Ultrason Ferroelectr Freq Control 2004;51:396–409.

Bhatia KS, Yuen EH, Cho CC, Tong CS, Lee YY, Ahuja AT. A pilot study evaluating real-time shear wave ultrasound elastography of miscellaneous non-nodal neck masses in a routine head and neck ultrasound clinic. Ultrasound Med Biol 2012;38:933–942.

Bouillard K, Nordez A, Hug F. Estimation of individual muscle force using elastography. PLoS One 2011;6:e29261.

Brandenburg JE, Eby SF, Song P, Zhao H, Brault JS, Chen S, An KN. Ultrasound elastography: The new frontier in direct measurement of muscle stiffness. Arch Phys Med Rehabil 2014;95:2207–2219.

Buchanan TS, Lloyd DG, Manal K, Besier TF. Neuromusculoskeletal modeling: Estimation of muscle forces and joint moments and movements from measurements of neural command. J Appl Biomech 2004;20:367–395.

Choi WJ, Kim HH, Cha JH, Shin HJ, Kim H, Chae EY, Hong MJ. Predicting prognostic factors of breast cancer using shear wave elastography. Ultrasound Med Biol 2014;40:269–274.
Cohen J. Weighted kappa: nominal scale agreement with provision for scaled disagreement or partial credit. Psychol Bull 1968;70:213–220.
Debernard L, Robert L, Charleux F, Bensamoun SF. Analysis of thigh muscle stiffness from childhood to adulthood using magnetic resonance elastography (MRE) technique. Clin Biomech 2011;26:836–840.
Debernard L, Robert L, Charleux F, Bensamoun SF. Characterization of muscle architecture in children and adults using magnetic resonance elastography and ultrasound techniques. J Biomech 2011;44:397–401.
Dresner MA, Rose GH, Rossman PJ, Muthupillai R, Manduca A, Ehman RL. Magnetic resonance elastography of skeletal muscle. J Magn Reson Imaging 2001;13:269–276.
Dutt V, Kinnick RR, Muthupillai R, Oliphant TE, Ehman RL, Greenleaf JF. Acoustic shear-wave imaging using echo ultrasound compared to magnetic resonance elastography. Ultrasound Med Biol 2000;26:397–403.
Eby SF, Song P, Chen S, Chen Q, Greenleaf JF, An KN. Validation of shear wave elastography in skeletal muscle. J Biomech 2013;46:2381–2387.
Eby SF, Cloud BA, Brandenburg JE, Giambini H, Song P, Chen S, LeBrasseur NK, An KN. Shear wave elastography of passive skeletal muscle stiffness: Influences of sex and age throughout adulthood. Clin Biomech 2015;30:22–27.
Edwards RG, Lippold OC. The relation between force and integrated electrical activity in fatigued muscle. J Physiol 1956;132:677–681.
Erdemir A, McLean S, Herzog W, van den Bogert AJ. Model-based estimation of muscle forces exerted during movements. Clin Biomech 2007;22:131–154.
Gennisson JL, Catheline S, Chaffaï S, Fink M. Transient elastography in anisotropic medium: Application to the measurement of slow and fast shear wave speeds in muscles. J Acoust Soc Am 2003;114:536–541.
Haen TX, Roux A, Soubeyrand M, Laporte S. Shear waves elastography for assessment of human Achilles tendon's biomechanical properties: An experimental study. J Mech Behav Biomed Mater 2017;69:178–184.
Hill AV. The heat of shortening and the dynamic constants of muscle. Proc R Soc B Biol Sci 1938;126:136–195.
Hirata K, Miyamotomikami E, Kanehisa H, Miyamoto N. Muscle-specific acute changes in passive stiffness of human triceps surae after stretching. Eur J Appl Physiol 2016;116:911–918.
Hug F, Tucker K, Gennisson JL, Tanter M, Nordez A. Elastography for muscle biomechanics: Toward the estimation of individual muscle force. Exerc Sport Sci Rev 2015;43:125–133.
Huijing PA. Muscle as a collagen fiber reinforced composite: A review of force transmission in muscle and whole limb. J Biomech 1999;32:329–345.
Huxley AF, Niedergerke R. Structural changes in muscle during contraction: Interference microscopy of living muscle fibres. Nature 1954;173:971–973.
Hylander WL, Ravosa MJ, Ross CF, Wall CE, Johnson KR. Symphyseal fusion and jaw-adductor muscle force: An EMG study. Am J Phys Anthropol 2000;112:469–492.
Itoh A, Ueno E, Tohno E, Kamma H, Takahashi H, Shiina T, Yamakawa M, Matsumura T. Breast disease: Clinical application of US elastography for diagnosis. Radiology 2006;239:341–350.
Kelly JP, Koppenhaver SL, Michener LA, Proulx L, Bisagni F, Cleland JA. Characterization of tissue stiffness of the infraspinatus, erector spinae, and gastrocnemius muscle using ultrasound shear wave elastography and superficial mechanical deformation. J Electromyogr Kinesiol 2017;38:73–80.
Kentaro C, Ryota A, Michiko D, Fukashiro S, Takahashi H. Reliability and validity of quantifying absolute muscle hardness using ultrasound elastography. PloS One 2012;7:e45764.
Kim SO, Lee SY, Jang SI, Park SJ, Kwon HW, Kim SH, Lee ES, Choi SK, Cho SH, Kim YM. Hepatic stiffness using shear wave elastography and the related factors for a Fontan circulation. Pediatr Cardiol 2018;39:57–65.
Koo TK, Guo JY, Cohen JH, Parker KJ. Relationship between shear elastic modulus and passive muscle force: An ex-vivo study. J Biomech 2013;46:2053–2059.
Koo TK, Guo JY, Cohen JH, Parker KJ. Quantifying the passive stretching response of human tibialis anterior muscle using shear wave elastography. Clin Biomech 2014;29:33–39.
Kot BC, Zhang ZJ, Lee AW, Leung VY, Fu SN. Elastic modulus of muscle and tendon with shear wave ultrasound elastography: Variations with different technical settings. PloS One 2012;7:e44348.
Kwak JY, Han KH, Yoon JH, Moon HJ, Son EJ, Park SH, Jung HK, Choi JS, Kim BM, Kim EK. Thyroid imaging reporting and data system for US features of nodules: A step in establishing better stratification of cancer risk. Radiology 2011;260:892–899.
Le SG, Nordez A, Andrade R, Hug F, Freitas S, Gross R. Stiffness mapping of lower leg muscles during passive dorsiflexion. J Anat 2017;230:639–650.
Leonardis JM, Desmet DM, Lipps DB. Quantifying differences in the material properties of the fiber regions of the pectoralis major using ultrasound shear wave elastography. J Biomech 2017;63:41–46.
Levinson SF, Shinagawa M, Sato T. Sonoelastic determination of human skeletal-muscle elasticity. J Biomech 1995;28:1145–1154.
Liu YL, Li GY, He P, Mao ZQ, Cao Y. Temperature-dependent elastic properties of brain tissues measured with the shear wave elastography method. J Mech Behav Biomed Mater 2017;65:652–656.
Lloyd DG, Besier TF. An EMG-driven musculoskeletal model to estimate muscle forces and knee joint moments in vivo. J Biomech 2003;36:765–776.
Maïsetti O, Hug F, Bouillard K, Nordez A. Characterization of passive elastic properties of the human medial gastrocnemius muscle belly using Supersonic shear imaging. J Biomech 2012;45:978–984.
Miyamoto N, Hirata K, Kanehisa H. Effects of hamstring stretching on passive muscle stiffness vary between hip flexion and knee extension maneuvers. Scand J Med Sci Sports 2015;27:99–106.
Modenese L, Phillips ATM. Prediction of hip contact forces and muscle activations during walking at different speeds. Multibody Syst Dyn 2012;28:157–168.
Mulabecirovic A, Mjelle AB, Gilja OH, Vesterhus M, Havre RF. Repeatability of shear wave elastography in liver fibrosis phantoms—Evaluation of five different systems. PLoS One 2018;13 e0189671.
Nightingale K, Mcaleavey S, Trahey G. Shear-wave generation using acoustic radiation force: In vivo and ex vivo results. Ultrasound Med Biol 2003;29:1715–1723.
Nordez A, Gennisson JL, Casari P, Catheline S, Cornu C. Characterization of muscle belly elastic properties during passive stretching using transient elastography. J Biomech 2008;41:2305–2311.
Nordez A, Hug F. Muscle shear elastic modulus measured using SuperSonic shear imaging is highly related to muscle activity level. J Appl Physiol 2010;108:1389–1394.
Oudry J, Chen J, Glaser KJ, Miette V, Sandrin L, Ehman RL. Cross-validation of magnetic resonance elastography and ultrasound-based transient elastography: A preliminary phantom study. J Magn Reson Imaging 2009;30:1145–1150.
Palmeri ML, Wang MH, Dahl JJ, Frinkley KD, Nightingale KR. Quantifying hepatic shear modulus in vivo using acoustic radiation force. Ultrasound Med Biol 2008;34:546–558.
Park JY, Lee HJ, Jang HW, Kim HK, Yi JH, Lee W, Kim SH. A proposal for a thyroid imaging reporting and data system for ultrasound features of thyroid carcinoma. Thyroid 2009;19:1257–1264.
Sarvazyan AP, Rudenko OV, Swanson SD, Fowlkes JB, Emelianov SY. Shear wave elasticity imaging: A new ultrasonic technology of medical diagnostic. Ultrasound Med Biol 1998;24:1419–1435.
Schless SH, Hanssen B, Cenni F, Baron L, Aertbeliën E, Molenaers G, Desloovere K. Estimating medial gastrocnemius muscle volume in children with spastic cerebral palsy: A cross-sectional investigation. Dev Med Child Neurol 2018;60:81–87.
Snyder WS, Cook MJ, Nasset ES, Karhausen RL, Howells GP, Tipton IH. Report of the Task Group on Reference Man. International

Commission on Radiological Protection (ICRP) Publ. 23. Oxford: Pergamon Press; 1975.
SuperSonic Imagine. SSIP01143, Revision 05A: Aixplorer user's guide. Aix-en-Provence: Author, 2016.
Tran D, Podwojewski F, Beillas P, Ottenio M, Voirin D, Turquier F, Mitton D. Abdominal wall muscle elasticity and abdomen local stiffness on healthy volunteers during various physiological activities. J Mech Behav Biomed Mater 2016;60:451–459.
Turgay E, Salcudean S, Rohling R. Identifying the mechanical properties of tissue by ultrasound strain imaging. Ultrasound Med Biol 2006;32:221–235.
Umegaki H, Ikezoe T, Nakamura M, Nishishita S, Kobayashi T, Fujita K, Tanaka H, Ichihashi N. The effect of hip rotation on shear elastic modulus of the medial and lateral hamstrings during stretching. Manual Ther 2015;20:134–137.
Urban MW, Nenadic IZ, Chen S, Greenleaf JF. Discrepancies in reporting tissue material properties. J Ultrasound Med 2013;32:886–888.
Weickenmeier J, Kurt M, Ozkaya E, Wintermark M, Pauly KB, Kuhl E. Magnetic resonance elastography of the brain: A comparison between pigs and humans. J Mech Behav Biomed Mater 2018;77:702–710.
Zhi H, Xiao XY, Yang HY, Wen YL, Ou B, Luo BM, Liang BL. Semi-quantitating stiffness of breast solid lesions in ultrasonic elastography. Acad Radiol 2008;15:1347–1353.
Ziai A, Menon C. Comparison of regression models for estimation of isometric wrist joint torques using surface electromyography. J Neuroeng Rehabil 2011;8:56–68.